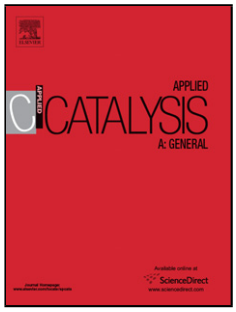

Title: Ni(II)–Mg(II)–Al(III) catalysts for hydrogen production from ethanol steam reforming: Influence of the Mg content

Author: Adriana Romero Matías Jobbágy Miguel Laborde Graciela Baronetti Norma Amadeo

PII: S0926-860X(13)00673-X
DOI: http://dx.doi.org/doi:10.1016/j.apcata.2013.10.054
Reference: APCATA 14548

To appear in: *Applied Catalysis A: General*

Received date: 24-5-2013
Revised date: 18-10-2013
Accepted date: 29-10-2013

Please cite this article as: A. Romero, M. Jobbágy, M. Laborde, G. Baronetti, N. Amadeo, Ni(II)ndashMg(II)ndashAl(III) catalysts for hydrogen production from ethanol steam reforming: Influence of the Mg content, *Applied Catalysis A, General* (2013), http://dx.doi.org/10.1016/j.apcata.2013.10.054

Ni(II)–Mg(II)–Al(III) catalysts for hydrogen production from ethanol steam reforming: Influence of the Mg content

Adriana Romero[a], Matías Jobbágy[b], Miguel Laborde[a], Graciela Baronetti[a], Norma Amadeo[a,*]

[a] Laboratorio de Procesos Catalíticos, Departamento de Ingeniería Química, Facultad de Ingeniería Ciudad Universitaria, (1428) Buenos Aires, Argentina

[b] INQUIMAE, Facultad de Ciencias Exactas y Naturales, Universidad de Buenos Aires, Pabellón II, Ciudad Universitaria, (1428) Buenos Aires, Argentina
*Corresponding autor: Fax: +54 11 4576 3241. E-mail addresses: norma@di.fcen.uba.ar, normaamadeo@yahoo.com.ar .

1. Introduction

During the last centuries, human civilization has solved the energy supply problem mainly on the bases of fossil sources of carbon and hydrocarbons and the associated technologies. In the last three decades there have been growing concerns about the shortage in energy supply in the world [1], which triggered the searching for alternative sources and technologies. Most of the chemical based alternatives consider hydrogen as an efficient energetic vector since it directly transforms chemical energy into electric current by means of fuel cells technology, releasing steam as the only product. However, hydrogen non-contaminant character depends on the nature of the raw material used as source. In this sense, steam reforming of ethanol, obtained from biomass, offers a true green alternative for H_2 production, due to its inherent renewable character, low toxicity (unlike methanol) and the fact that it can be obtained virtually sulphide-free [2,3]. Ethanol has relatively high hydrogen content and in presence of water, is capable of producing 6 mol of H_2 per mol of ethanol:

$$C_2H_5OH + 3H_2O \rightarrow 2CO_2 + 6H_2 \quad (1)$$

From a thermodynamic viewpoint, reforming reaction is highly favorable, however it competes with multiple side reactions [2,4] and in general, the outflow from the reactor contents a wide range of liquids and gaseous products. Different catalytic systems have been proved to be effective with variable hydrogen selectivities [1-11]. Ni catalysts have been widely utilized in reforming of hydrocarbons because it promotes the rupture of the C–C bonds, achieving high activity [11-14]. Noble-metal-catalysts (Rh, Pt, and Pd) also present high activity and selectivity [9], however their high cost limits their high-scale-use, in contrast to nickel based ones.

Steam reforming reaction takes place on the surface of a solid catalyst. For this process usually nickel supported catalysts are used. Water adsorbs preferentially on the catalysts support, formulated to allow mobility for oxygen species, originated from water dissociation, adsorbed on its surface, while hydrocarbon molecules adsorb preferentially on the metal surface (metallic nickel), and the steam reforming reaction takes place at the metal–support interface [15-19].

In order to prevent undesired carbon formation, which is the principal cause of poisoning in Ni based catalysts used in this process, ternary Ni(II)–Mg(II)–Al(III) oxides were proposed, where the presence of Mg(II) disfavor this undesired product [20].

Catalyst characteristics are determined by their physical-chemistry, structural and textural properties, as they are: active area, metal particle size, metal dispersion and reducibility. These properties depend on metal–support interaction, and they could be established on different stages of catalyst synthesis and thermal treatment. For example, varying precursor material composition, preparation method and/or activation (calcination, reduction) [1,21,22].

Thermal decomposition of crystalline monophasic precursors as Me(II)-Al(III)-based layered double hydroxides (LDHs) leads to complex oxides, ideally composed of highly dispersed MeO and $MeAl_2O_4$ mixtures. [23-25]. However, the aforementioned stoichiometric phases are only achieved after massive demixing at high temperatures, an ill crystallized non-stoichiometric phases are expectable at intermediate annealing [26]. Moreover, in a previous work, we concluded that thermal treatments of Ni(II)-Al(III) LDHs lead to synergetic effects between the elements in mixed oxide structures, and after appropriate activation treatment, give rise to well dispersed metal particles like a supported metal catalysts, with the possibility of controlling metal–support interaction during the synthesis and treatment stages [22].

The aim of this work is to study in which extent the partial replacement of Ni(II) by Mg(II) in a family of LDHs affect the nature of their mixed oxides in terms of their reducibility, activity, product distribution and carbon deposition during ethanol steam reforming process.

2. Experimental

2.1. Synthesis and characterization

Mother solutions of Al(III), Ni(II) and Mg(II) nitrates (0.5 mol/l, each) were prepared dissolving $Al(NO_3)_3.9H_2O$, $Ni(NO_3)_2.6H_2O$ and $Mg(NO_3)_2.6H_2O$ in distilled water, respectively. Catalyst precursors were prepared by homogeneous precipitation method based on urea hydrolysis [22], for which solutions containing urea–Ni(II)–Mg(II)–Al(III) in proper ratios for each catalyst; were aged at 363K during 24 h in PP bottles. The reaction was quenched submitting the bottles into ice-bath. The precipitated precursors were centrifuged, washed with cold distilled water and dried at 343K. Total concentrations for the starting solutions of urea and cations [Ni(II) + Mg(II) + Al(III)] were 0.5 mol/l and 5.0 x 10^{-2} mol/l, respectively. Initial molar ratio of [Ni(II) + Mg(II)]/Al(III) were 2 [27]. The catalysts were named "HT*x*", being *x* = molar ratio Mg(II)/Ni(II), as indicated in Table 1. After that, the precursors were reduced with a heating ramp of 10 K/min up to 993K, holding such temperature for 2 h, in pure hydrogen flow of 100 ml/min. An "R" letter was added to the nomenclature for reduced samples.

Samples were characterized by ICP chemical analysis, thermogravimetric analysis (TGA), sorptometry (S_{BET}), H_2 chemisorption, powder X-ray diffraction (PXRD), X-ray photoelectronic spectroscopy (XPS) and temperature programmed reduction (TPR). After catalytic performance, catalysts were analyzed by temperature programmed oxidation (TPO), in order to quantify carbon deposits.

BET surface area was obtained in a Micromeritics ASAP 2020equipment. Reduced Ni area was evaluated by H_2 static volumetric chemisorption measurements in a Micromeritics AutoChem II 2920 equipment. Ni metallic area was calculated assuming a Ni/H = 1 stoichiometry and that a Ni atom occupies 6.45Å^2. Solid composition was analyzed in a Sequential Plasma Spectrometer ICP-AES Shimadzu 1000 III. Thermogravimetric studies were carried out in a Shimadzu TGA-51H equipment, using a heating ramp of 10 K/min in air flow of 50 cm^3/min. Solids were characterized by PXRD in a Siemens D 5000 equipment (radiation Cu Kα).

XPS analysis was carried out in a multi-technical system (SPECS) which has a hemispheric analyzer PHOIBOS 150 operating in fix analyzer transmission mode (FAT). Spectra were acquired with a step energy of 30 eV, using Mg Kα radiation X-ray source operated at 200W and 12 kV. Work pressure in analysis chamber was lower than 5 x 10^{-9} mbar. Spectra quantification was made by Casa XPS Software [28] using the analyzer's transmission function appropriated values of the Scofield factors. Curves were deconvolucionated by Gaussian and Lorentzian-type functions and Shirley-type background no-lineal subtraction. Binding energy values were corrected using the aluminium oxide Al 2p line at 74.3 eV as reference [29].

TPR experiments were performed in a Micromeritics AutoChem II 2920 equipment, using an amount of sample of 100 mg, N_2/H_2 flow of 100 ml/min (molar composition 98/2%) and a heating ramp of 10K/min in the range of 293-1173K. Previously, the precursor was calcined in oven at 623K during 1 hour in order to avoid anion reduction to occur simultaneously with the Ni(II) reduction. Previous runs with different amounts of pure CuO were carried out in order to quantify the detector signal. TPO experiments were carried out in the same equipment than TPR ones, with the following conditions: an amount of 20 mg of sample was pretreated in an Argon flow of 50

ml/min from 298 to 573K, with a ramp of 20K/min, in order to eliminate any adsorbate which may interfere with the results. After that, the sample was cooled to 323K. TPO study was carried out from 323 to 1073K, with a ramp of 10K/min, in an Argon/Air flow of 50 ml/min (90/10% molar). Both TPR and TPO studies were carried out with Mass Spectrometry on line, in order to detect H_2, H_2O, CO and CO_2 species. It was utilized a ThermoStar TM Pfeiffer Vacuum equipment.

2.2. Catalytic performance

Experimental equipment used for catalytic evaluation consists of a quartz tubular reactor (Ø = 9.2 mm) heated in electric oven at the reaction temperature, which is monitored by a thermocouple placed inside the reactor. The ethanol and water feed is pumped with a syringe pump and evaporated before the entrance of the reactor, using nitrogen as carrier. The vaporized current is diluted with argon at the entrance of the reactor. Inlet and outlet composition analysis were carried out by GC in an Agilent Technologies 6890N equipment.

Ethanol conversion and product yields are defined as follows:

$$X = (y^{o}_{EtOH}-y^{s}_{EtOH})/y^{o}_{EtOH} \qquad Y_i = (y^{s}_{i}-y^{o}_{i})/y^{o}_{EtOH}$$

Where y^o: molar fraction in the inlet;
y^s: molar fraction in the outlet.

Two series of experiences were carried out. In all experiences, the operation conditions were chosen to prevent mass transfer limitations and guarantee isothermal conditions.

First, in order to study the effect of the Mg content over the activity and yields of the catalysts, the operative conditions were: catalyst mass: 8.0 mg; reaction temperature: 823K, water/ethanol molar ratio: 5.5, inert flow: 350 ml/min. The catalyst was diluted 1:10 with an inert solid. These conditions assured ethanol conversion to be lower than 100%.

Then, we have studied the effect of the Mg content over the carbon deposit on the catalyst, employing the following operative conditions: catalyst mass: 30.0 mg; reaction temperature: 923K, water/ethanol molar ratio: 5.5, inert flow: 400 ml/min. There was no dilution of the catalyst. After that, the samples were analyzed by TPO.

3. Results and discussion

Table 1 shows the chemical composition and specific surface for the samples. It can be seen that specific surface increases when Mg content does [30].

In the Figure 1 it can be observed PXRD spectra of precursors with different Mg content, all samples show characteristic signals of LDH. Peak sharpness (directly related to crystallinity) increases when Mg(II) content does [31].The main interbasal reflections (0 0 3), (0 0 6), in addition to the characteristic (1 1 0) and (1 1 3) reflections close to 2θ= 60º; indicate the presence of crystalline carbonate-intercalated hydrotalcite-like structure [32]. There is no evidence of $Ni(OH)_2$, $MgCO_3$nor AlO(OH) phase segregation [27,33].

Thermal decomposition occurs in two endothermic steps, typical for LDHs [23]. The first step, the transition is a constant weight loss in the range of 300 to 500K, which corresponds to reversible loss of interlaminar water, without structure collapse. The second step, between 500 and 700K, corresponds to irreversible dehydroxylation of brucitic layers and loss of carbonate anions.

TGA results for the sample without Mg (HT0.00) were reported in a previous work [13]. Figure 2 shows the obtained results in thermal decomposition. Total weight loss in % was between 30 and 37% for all samples, confirming the LDH nature of precursors, and these results were taking into account for further calculations. As we reported in a previous work [22], the evolution of thermal decomposition presents the same pattern, regardless of the study being carried out in oxidizing or reducing atmosphere [34].

In Fig. 3 PXRD patterns for all reduced samples are shown. In order to study the evolution of the structure during thermal treatment, the pattern of the precursor HT0.33 calcined at 973K (700ºC) was included (first pattern from below, HT0.33-C700).
After thermal decomposition, the initial structure collapses because of the loss of carbonates (decarboxylation) and hydroxyl groups (dehydration), transforming the solid into an oxide mixture. The sample HT0.33-C700 pattern shows characteristic reflections of NiO (Bunsenite, JCPDS 22-1189); because MgO (JCPDS 4-0829) has a similar NaCl-type structure, observed reflections at high angles could be consistent with $Ni_{1-q}Mg_qO$ solid solution. Since characteristic reflections of NiO, MgO and $Ni_{1-q}Mg_qO$ solid solution are very close, they are impossible to distinguish at low values of 2θ [35-39]. It has to be noticed that the inclusion of Al(III) in the lattice also affects these reflections, hindering the distinction of separated phases.
After reductive activation, all the precursors evolved into a metallic Ni phase (JCPDS 4-0850). Additional low intensity reflections at 2θ = 36,3; 59,5 and 65,3º were detected, suggesting incipient formation of a spinel-like phase (JCPDS 10-0339 $NiAl_2O_4$, 21-1152 $MgAl_2O_4$); which is expected, given the abundant presence of Al(III) in the solid. Previous reports based on neutron diffraction studies indicate that such mixed phases crystallize in an incipient way at 923K [40], while massive segregation (demixing) of stable phases takes place at 1273K [41].

TPR profiles for precursors with different ratios Mg/Ni are compared in Figure 4. It can be seen two broad peaks. According to Mass Spectrometer equipment monitoring on line, the first peak, at low temperature (430-630K), corresponds to the reduction of carbonate anions, which are not totally eliminated during pretreatment (heat in air at 623K for 60 minutes) [42]. It is remarkable that this event shifts to lower temperatures when Ni content increases. It is possible that at these low temperatures, the reduction of very small superficial particles of Ni has begun, having a catalytic effect on the reduction of nearby carbonates [33]. The second event, a very broad peak, (650-1150K) corresponds to the reduction of Ni(II) species associated to mixed oxides [41,43].
Quantitative analysis of the TPR profiles showed that Ni has been reduced between 86 and 97%, as presented in Table 2.
In order to identify the nature of these Ni(II) species in the second event, a peak fitting of the profiles was made. Figure 5 shows these results, which had an accuracy of R^2=0.997.

It can be seen that, for both fitting peaks (α and β), maximum H_2 consumption slightly shifts to higher temperatures as Mg(II) content increases. This fact is related to a stronger interaction of Ni(II) atoms with neighboring cations (see Table 2). It is known that a higher Mg(II) proportion makes Ni(II) less reducible, thus maximum H_2 consumption moves to higher temperatures [24,32,38].
According to the literature, peak α can be assigned to the reduction of Ni(II) in $Ni_{1-q}Mg_qO$ matrix [35-38], and peak β correspons to Ni(II) in a non-stoichiometric spinel-like phase [44,45],

confirmed by PXRD. Particularly, this spinel-like phase competes for divalent cations, taking up preferably Mg(II), and then Ni(II) when necessary [22].

On the other hand, the performance of the catalysts was tested in the ethanol steam reforming reaction. Figures 6, 7 and Table 3 show the catalytic results.
The highest conversion is obtained with the catalyst HT0.00, as shown in Figure 6. With increasing Mg(II) content, at the beginning the conversion diminishes, reaching a minimum, then increases a little to remain constant.
Hydrogen, CO and CO_2 yields have a similar behavior, after a minimum for Mg/Ni = 0.04, they remain constant at 70, 20 and 55% respectively.
Methane yield kept constant and lower than 3% (Figure 7) for all samples. Acetaldehyde yield stabilizes fewer than 10%. Ethylene yield shows higher values (almost 30%) for samples with low Mg content, but it decreases abruptly to values under 1% when Mg content increases.
Several authors consider ethylene as one of the principal responsible for coke deposition in steam reforming [46-49] and attribute to Mg(II) the capacity of giving higher mobility to anions OH^- and, thus, favoring ethanol dehydrogenation to acetaldehyde instead of dehydration to ethylene [1,30].
The sample HT0.33 has the best results set: high conversion (about 70%), the highest H_2 yield (82%) and the lowest ethylene and acetaldehyde yields.

In order to study the nature of the active sites for all catalysts, it was analyzed the H_2 yield per m^2 of metallic surface (parameter related with intrinsic activity). For this purpose, metallic area and active particle size were measured by H_2 chemisorption. The obtained results are indicated in Table 3. In this regard, as Mg content increases, Ni area (m^2/g_{cat}) decreases [30]. However, Ni metallic area per g_{Ni} remains constant, which indicates that Mg(II) content does not affect the metallic Ni dispersion.

H_2 yield per m^2 of metallic surface is shown in the last column of Table 3 and in Figure 8 as a function of %w Ni(II). It can be seen that the catalysts present several active sites with different intrinsic activity. However, Mg(II) content does not affect uniformly the nature of the active sites: the samples with low Mg(II) content present low intrinsic activity (Mg/Ni=0 up to 0,33); on the other hand, the samples with higher Mg(II) content present higher intrinsic activity (Mg/Ni=0,33 to 1,57).It seems to be a break point in the tendency for the sample HT0.33.

Besides, when TPR % α area (related to % $Ni_{1-q}Mg_qO$ solid solution present in the sample) is analyzed in Figure 8, both tendencies observed for intrinsic activity are present. In a previous work [22] we had proposed a model to explain in a schematic approach the structural and textural changes in the surface for Ni-rich samples (Mg/Ni = 0 up to 0,33) when they were submitted to different thermal treatments.
According to this model, during the thermal decomposition a complex phase segregation process takes place, in which the involved cations redistribute in order to reach their correspondent stable, commonly stoichiometric, oxides [50-52], before the birth of metallic Ni particles, when reducing atmospheres are employed.
The rate of segregation and the observed intermediate phases are strongly dependent on the nature of the involved cations; in the particular case of the ternary Ni(II)–Mg(II)–Al(III) LDHs, the starting oxide can be described as an ill crystallized spinel-like phase, in which all the cations share a single cubic oxygen framework. While Mg(II) and Al(III) can occupy either tetrahedral or octahedral positions within it, Ni(II) cations are exclusively placed at octahedral ones, irrespective

of the Ni(II) to Mg(II) ratio [39]. With further thermal treatment, the parent spinel-like metastable phase splits into two stable phases (demixing). In Ni-rich samples (Mg/Ni = 0 to 0,33) it is expected in the total demixing scenario, the segregation of pure NiO and ternary $Ni_{1-p}Mg_pAl_2O_4$ spinel, assuming that Mg(II) cations preferentially accumulate in the latter phase, in accordance with a previous report [53], made up with all the available Al(III) in the hydroxycarbonate precursors. Equations 1 and 2 show this evolution.

Equation1: Decomposition

$$Ni_xMg_yAl_z(OH)_2(CO_3)_{\frac{z}{2}}.nH_2O \rightarrow sl - Ni_xMg_yAl_zO_{1+\frac{z}{2}} + \frac{z}{2}CO_2 + (n+1)H_2O$$

$$x + y + z = 1$$

Equation 2: Demixing (for Ni-rich samples)

$$sl - Ni_xMg_yAl_zO_{1+\frac{z}{2}} \rightarrow \frac{z}{2}Ni_{\left(1-\frac{2y}{z}\right)}Mg_{\left(\frac{2y}{z}\right)}Al_2O_4 + \left(\frac{2y}{z} + x - 1\right)NiO$$

However, according to the presented model, the second group of samples (Mg/Ni = 0,33 to 1,57) has a different behavior. In the total demixing scenario for these Mg-rich samples, it is expected the segregation of pure $MgAl_2O_4$ spinel and $Ni_{1-q}Mg_qO$ solid solution. In the oxide phase, only part of the Ni(II) present would be reducible, depending of the strength of the interaction Ni(II)-Mg(II), since both cations form a solid solution oxide. In order to study this possibility, an XPS study was made for the sample HT1.57 in its reduced form. It was found that surface molar fraction of Al(III), Mg(II) and Ni(II) was 0.54, 0.41 and 0.05 respectively. In comparison to the bulk results (shown in Table1), it is observed that the surface becomes poor in Ni(II), indicating a spinel surface coverage of about 85% of the corresponding theoretical composition lines. Equations 3 and 4 explain this behavior. Figure 9 shows the evolution of the solids according to Mg(II) content.

Equation 3: Decomposition

$$Ni_xMg_yAl_z(OH)_2(CO_3)_{\frac{z}{2}}.nH_2O \rightarrow sl - Ni_xMg_yAl_zO_{1+\frac{z}{2}} + \frac{z}{2}CO_2 + (n+1)H_2O$$

$$x + y + z = 1$$

Equation 4: Demixing (for Mg-rich samples)

$$sl - Ni_xMg_yAl_zO_{1+\frac{z}{2}} \rightarrow \frac{z}{2}MgAl_2O_4 + \left(x + y - \frac{z}{2}\right)Ni_{1-q}Mg_qO$$

$$q = \frac{y - \frac{z}{2}}{x + y - \frac{z}{2}}$$

The two observed tendencies indicate that in the first group (Ni-rich samples), reducible Ni(II) (the active phase in steam reforming) comes from the NiO phase, meanwhile in the second group (Mg-rich samples), comes from the $Ni_{1-q}Mg_qO$ solid solution phase. The model predicts a break point in the behavior, for the case of the solid having just enough Mg(II) to form a pure $MgAl_2O_4$ spinel and NiO phases. This is in good agreement with our characterization results. The presence of different environment for the active sites in the samples is reflected by the results of activity in steam reforming. The samples with low Mg(II) content present a mixed spinel-like phase, $Mg_xNi_{1-x}Al_2O_4$, which would be more acidic than pure $MgAl_2O_4$ [9], presented in the samples with higher Mg(II) content. This fact favors the dehydration of ethanol to ethylene in samples with low Mg(II) content.

Besides, it is noticeable that TPR α and β events shift at lower temperatures when Mg(II) content increases, without showing a break point (see Table 2). This must be due to the fact that during thermal treatment, reduction occurs simultaneously with the demixing (phase segregation).

Beyond the textural model depicted herein, low yields of hydrogen for the Ni rich samples results from undesired C_2 products as ethylene and acetaldehyde, which subsequently drive to coke formation. This fact could obey to the occurrence of Al(III) acid sites; their presence was documented for related solids obtained by the straight decomposition of Mg-Al LDH and Ni-Al LDH [54]. The latter, in particular reflected a delayed crystallization of $NiAl_2O_4$, respect to $MgAl_2O_4$, leaving significant amounts of surface amorphous alumina, silent to PXRD inspection, in which acid Al(III) sites are likely. The aforementioned behavior seems to remain, at least partially in our samples, particularly on those in which Ni ions are more abundant than Mg ones within the parent LDH lattice.

On the other hand, it is well known that the addition of Mg(II) considerably improves the resistance of the catalyst to the coke deposition. In order to analyze this effect, kinetic experiments have been carried out using a mass of catalyst of 30 mg, increasing the residence time, and reaching total conversion. Thus, by increasing the permanence time of carbon precursors in the reactor, it favors coke deposition.

TPO technique was applied on these used samples in order to carry out a qualitative analysis about the type and amount of coke formed on the bed. Figure 10 and Table 4 show these results.

A pronounced diminish of the CO_2 amount is observed when proportion Mg/Ni increases. These results are according with Melo et al. [1,30] who claims that higher Mg(II) content leads to a higher capacity for water adsorption-dissociation and oxygen species mobility. All these characteristics produce materials with better resistance to carbon deposition. They conclude that resistance to carbon deposition increases when metal dispersion increases and metallic particle size decreases. Higher Mg(II) content leads to smaller metallic area and metallic particles. Carbon growing on Ni^o particle is enhanced when particle size is greater. Our results support this fact, since the sample with lowest particle size presents the lowest coke deposition.

All profiles show an only CO_2 peak. This fact leads to think that an only type of coke is formed in the bed. Therefore, basing in Kitiyanan et al. results [55], we can conclude that this only type of coke is a mixture of monotubular and multitubular nanofibers.

This type of coke doesn't lead to an activity loss, but a bed porosity decrease and thus an increase in the reactor pressure.

The obtaining of an only CO_2 peak, and no CO peak, indicates a lineal relation between gasified CO_2 amount and formed coke amount on the catalyst surface during reaction.

Taking this into account, it is possible to conclude that an increase in the Mg(II) content in the precursor leads to a decrease in the coke deposition during reaction.

4. Conclusions

The Ni(II)–Mg(II)–Al(III) LDH obtained by homogeneous precipitation urea method, after a proper thermal treatment resulted in an active catalyst for the ethanol steam reforming. The results show that addition of a basic cation such as Mg(II) redounds favorably in the resistance to carbon deposition. However, in terms of activity and product distribution in ESR reaction, there is an optimal Mg/Ni ratio = 0,33, which shows the best results. This is related to the fact that when Mg/Ni ratio varies, the interaction of Ni^o in the oxide matrix changes, and so it does the nature of the active sites.

It can be concluded from this report that the appropriate ratio between the cations Ni(II)–Mg(II)–Al(III), and after a proper reduction treatment, would allow to control the interaction of the Ni^o active centers with the environment and the solids structure, redounding in an improved activity, H_2 yield and resistance to carbon deposition.

5. Acknowledgements

To ANPCyT, CONICET and UBA, for the economic support. Also, thanks are given to ANPCyT for Grant PME 8-2003 to finance the purchase of the UHV Multi Analysis System. MJ also acknowledge CONICET for the PIP 5215 project financial support. The careful and devoted revision provided by the expert reviewer is deeply appreciated by the authors.

6. References

[1] F. Melo, N. Morlanés, Cat. Today 133-135 (2008) 383-393.
[2] J. Comas, F. Mariño, M. Laborde, N. Amadeo, Chem. Eng. J. 98 (1–2) (2004) 61-68.
[3] F. Mariño, E. Cerrella, S. Duhalde, M. Jobbágy, M. Laborde, Int. J. Hydrogen Energy 23 (1998) 1095-1101.
[4] S. Cavallaro, Energy Fuels 14 (2000) 1195-1199.
[5] J. Llorca, N. Homes, J. Sales, P. Ramírez de la Piscina, J. Catal. 209 (2002) 306-317.
[6] F. Mariño, G. Baronetti, M. Jobbágy, M. Laborde, Appl. Catal. A: Gen. 238 (2003) 41-54.
[7] J. Llorca, P. Ramírez de la Piscina, J.A. Delmon, J. Sales, N. Homes, Appl. Catal. B: Environ. 43 (2003) 355-369.
[8] S. Cavallaro, V. Chiodo, S. Freni, N. Mondillo, F. Frusteri, Appl. Catal. A: Gen. 249(2003) 119-128.
[9] F. Aupretre, C. Descorme, D. Duprez, D. Casanave, D. Uzio, J. Catal. 233 (2005) 464-477.
[10] A. Akande, R. Idem, A. Delai, Appl. Catal. A: Gen. 287 (2005) 159-175.
[11] A. Haryanto, S. Fernando, N. Murali, S. Adhikari, Energy Fuels 19 (2005) 2098-2106.
[12] S. Velu, K. Suzuki, M. Vijayaraj, S. Barman, C.S. Gopinath, Appl. Catal. B: Environ. 55 (2005) 287-299.
[13] V. Mas, M.L. Dieuzeide, M. Jobbágy, G. Baronetti, N. Amadeo, M. Laborde, Catal. Today 133-135 (2008) 319-323.
[14] F. Frusteri, S. Freni, V. Chiodo, L. Spadaro, O. Di Biasi, G. Bonura, S. Cavallaro, Appl. Catal. A: Gen. 270 (2004) 1-7.
[15] D.L. Trimm, A.A. Adesina, Praharso, N.W. Cant, Catal. Today 93–95 (2004) 17-22.
[16] X. Wang, R.J. Gorte, Appl. Catal. A: Gen. 224 (2002) 209-218.
[17] Q. Ming, T. Healey, L. Allen, P. Irving, Catal. Today 77 (2002) 51-64.
[18] J.R. Rostrup-Nielsen, Catalysis science and technology, in: J.R. Anderson, M. Bouduart (Eds.), Catalytic Steam Reforming, vol. 5, Springer-Verlag editions, 1984 (Chapter 1).
[19] J.R. Rostrup Nielsen, J. Sehested, Adv. Catal. 47 (2002) 65-138.
[20] J.R. Rostrup-Nielsen, J. Catal. 33 (1974) 184-201.
[21] D. Tichit, B. Coq, Cattech 7 (2003) 206-217.
[22] A. Romero, M. Jobbágy, M. Laborde, G. Baronetti, N. Amadeo, Catal. Today 149 (2010) 407-412.
[23] F. Cavani, F. Trifirò, A. Vaccari, Catal. Today 11 (1991) 173-301.
[24] A. Vaccari, Appl. Clay Sci. 14 (1999) 161-198.
[25] T. Borowieki, Appl. Catal. A: Gen. 4 (1987) 207-220.

[26] Johnsen, Rune E.; Norby; J. Phys. Chem. C 113, 44 (2009) 19061-19066.
[27]Y.Yang, X. Zhao, F. Zhang; Chem. Mater. 24 (2012)81-87.
[28] N. Fairley, Casa XPS Software, 2.3.13 Version, 2007-12-03.
[29] C. Wagner, A. Naumkin, A. Kraut-Vass, J. Allison, C. Powell, J. Rumble, NIST X-Ray Database 20, Version 3.4 (Web version). NIST Standard Reference database 20, National Institute of Standars and Tecnology, Gaintherburg, USA.
[30] F. Melo, N. Morlanés, Catal. Today 107–108 (2005) 458–466.
[31]M.J. Holgado, V. Rives, M.S. San Román, Appl. Catal. A: General 214 (2001) 219-228.
[32] V. Rives, M.A. Ulibarri, Coordin. Chem. Rev. 181 (1999) 61-120.
[33] G.J. de, A.A. Soler-Illia, M. Jobbágy, A.E. Regazzoni, M.A. Blesa, Chem. Mater. 11 (1999) 3140-3146.
[34] O. Lebedeba, D. Tichit, B. Coq, Appl. Catal. A: Gen. 183 (1999) 61-71.
[35] O.W. Pérez-López, A. Senger, N.R. Marcilio, M.A. Lansarin, Appl. Catal. A: Gen. 303 (2006) 234-244.
[36] J. Feng, Y. Ding, Y. Guo, X. Li, W. Li, Fuel 109 (2013) 110-115.
[37] M. Kong, Q. Yang, J. Fei, X. Zheng, Int. J. Hydrogen Energy 37 (2012) 13355-13364.
[38] M. Kong, Q. Yang, W. Lu, Z. Fan, J. Fei, X. Zheng,T.D. Wheelock, Chinese J. Catal. 33 (2012) 1508-1516.
[39] Y. Wang, H. Liu, B. Xu, J. of Mol. Catal. A: Chem. 299 (2009) 44-52.
[40] M. Gazzano, W. Kagunya, D. Matteuzzi, A. Vaccari, J. Phys. Chem. B 101 (23) (1997) 4514-4519.
[41] O. Clause, M. Gazzano, F. Trifirò, A. Vaccari, L. Zatorski, Appl. Catal. 73 (2) (1991) 217-236.
[42] T. Tichit, F. Medina, B. Coq, R. Dutartre, Appl. Catal. A: Gen. 159 (1997) 241-258.
[43] J. Rodríguez, J. Hanson, A. Frenkel, J. Kim, M. Pérez, J. Am. Chem. Soc. 124 (2002) 346-354.
[44] K. Park, K.Y. Kim, L.Lu, T.H. Lim, S.A. Hong, H.I. Lee, Fuel Cells 07, 3 (2007) 211-217.
[45] A. Penkova, L. Bobadilla, S. Ivanova, M.I. Domínguez, F. Romero-Sarria, A.C. Roger, M.A. Centeno, J.A. Odriozola, Appl. Catal. A: Gen. 392 (2011) 184-191.
[46] A.J.Vizcaíno, P.Arena, G.Baronetti, A.Carrero, J.A.Calles, M.A.Laborde, N.Amadeo, Int. J. Hydrogen Energy 33 (2008) 3489-3492.
[47] A.Carrero, J.A.Calles, A.J.Vizcaíno, Chem. Eng. J. 163, 3 (2010) 395-402.
[48] F.Aupretre, C.Descorme, D.Duprez, D.Casanave, D.Uzio, J. Catal. (2005) 464-477 .
[49] H.Wang, Y.Liu, L.Wang, Y.N.Qin, Chem. Eng. J. 145 (2008) 25-31.
[50] M. Bellotto, B. Rebours, O. Clause, J. Phys. Chem.-US 100 (20) (1996) 8527-8534.
[51] M. Bellotto, B. Rebours, O. Clause, J. Phys. Chem.-US 100 (20) (1996) 8535-8542.
[52] E. Sileo, M. Jobbágy, C. Paiva-Santos, A. Regazzoni, J. Phys. Chem. B 109 (2005)10137-10141.
[53] F. Basile, L. Basini, M. D'Amore, G. Fornasari, A. Guarinoni, D. Matteuzzi, G. Del Piero, F. Trifirò, A. Vaccari, J. Catal. 173 (1998) 247-256.
[54] B. Rebours, J.B.D. De La Caillerie, O. Clause, J. Am. Chem. Soc. 116 (5) (1994) 1707-1717.
[55] B. Kitiyanan, W.E.Alvarez, J.H.Harwell, D.E.Resasco, Chem. Phys. Lett. 317 (2000) 497-503.

Highlights

- Mg-Ni-Al hydrotalcites were prepared by homogeneous precipitation method with urea.
- Derived mixed oxides were studied as catalysts in ethanol steam reforming.
- A thermal evolution model for the solids is proposed from characterization results.
- Mg/Ni molar ratio = 0.33 gives the best results of activity and carbon deposition.

*Graphical Abstract (for review)

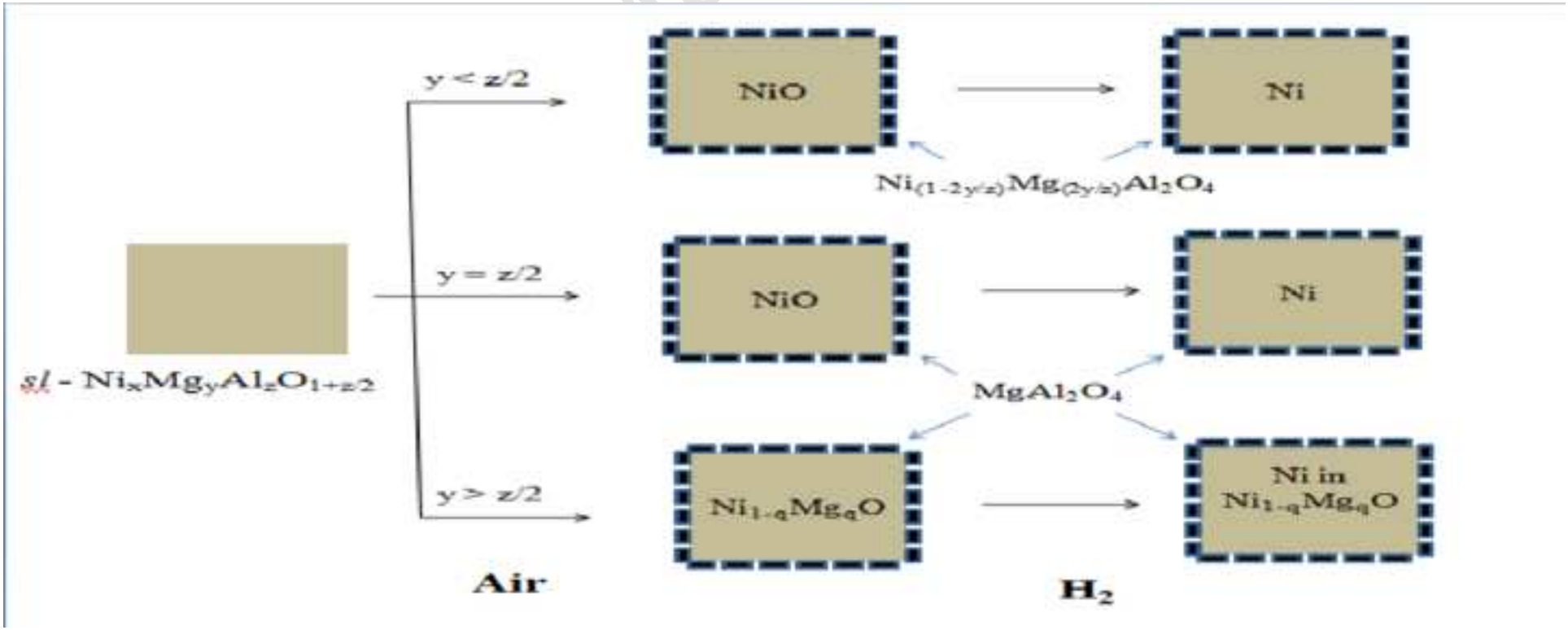

Caption to Figures

Figure 1. PXRD spectra of precursors.

Figure 2. Thermal decomposition.

Figure 3. PXRD spectra of reduced samples.(▼) NiO; (■) Ni^0; (◊) spinel-like phase.

Figure 4. TPR profiles for the samples with different ratios Mg/Ni.

Figure 5. 2nd TPR event fitting.

Figure 6. Ethanol conversion and H_2, CO and CO_2 yields.

Figure 7. Methane, ethylene and acetaldehyde yields.

Figure 8. Intrinsic activity (H_2 yield per metallic area unit) and TPR % α area vs. %w Ni.

Figure 9. Scheme of the evolution of the precursors during thermal treatment, as a function of Mg(II) content.

Figure 10. TPO profiles of different samples.

Caption to Tables

Table 1. Chemical composition and specific surface of precursors.

Table 2. Ni reducibility for all precursors.

Table 3. Chemisorption data and intrinsic conversion.

Table 4. TPO results.

Sample	% w Ni	LDH Formula	Sg (m^2/g_{cat})
HT0,00	57,67	$Ni_{0.69}Al_{0.31}(OH)_2(CO_3)_{0.15}.nH_2O$	96,8
HT0,04	60,08	$Ni_{0.72}Mg_{0.03}Al_{0.26}(OH)_2(CO_3)_{0.13}.nH_2O$	106,6
HT0,16	50,32	$Ni_{0.60}Mg_{0.10}Al_{0.30}(OH)_2(CO_3)_{0.15}.nH_2O$	145,4
HT0,33	45,41	$Ni_{0.51}Mg_{0.17}Al_{0.32}(OH)_2(CO_3)_{0.16}.nH_2O$	173,2
HT0,72	34,97	$Ni_{0.28}Mg_{0.39}Al_{0.33}(OH)_2(CO_3)_{0.17}.nH_2O$	201,0
HT1,20	30,18	$Ni_{0.30}Mg_{0.37}Al_{0.33}(OH)_2(CO_3)_{0.17}.nH_2O$	216,3
HT1,57	23,12	$Ni_{0.26}Mg_{0.41}Al_{0.33}(OH)_2(CO_3)_{0.17}.nH_2O$	209,3

Table 1.

Sample	% red Ni	Tα (K)	Tβ (K)	α/(α+β) area ratio
HT0.00	94	838	968	0,49
HT0.04	97	818	978	0,50
HT0.16	95	848	1003	0,37
HT0.33	93	840	1013	0,26
HT0.72	94	858	1023	0,24
HT1.20	86	880	1058	0,19
HT1.57	90	900	1063	0,18

Table 2.

Sample	A_{Ni} (m^2/g_{cat})	A_{Ni} (m^2/g_{Ni})	dp (nm)	Y_{H2}/m^2 metallic Ni
HT0.00	17,67	30,65	18,3	2,91
HT0.04	18,91	31,47	17,8	1,43
HT0.16	18,41	36,58	15,4	2,51
HT0.33	14,70	32,38	17,4	5,60
HT0.72	14,99	42,85	13,1	5,06
HT1.20	10,45	34,63	16,2	6,86
HT1.57	9,54	41,25	13,6	7,23

Table 3.

Sample	CO_2 maximum temperature	CO_2 area (x100)	area/w%Ni (relative to HT0.00)
HT0.00	875	8,857	100%
HT0.33	867	3,612	52%
HT0.72	860	1,827	34%
HT1.57	832	0,519	15%

Table 4.

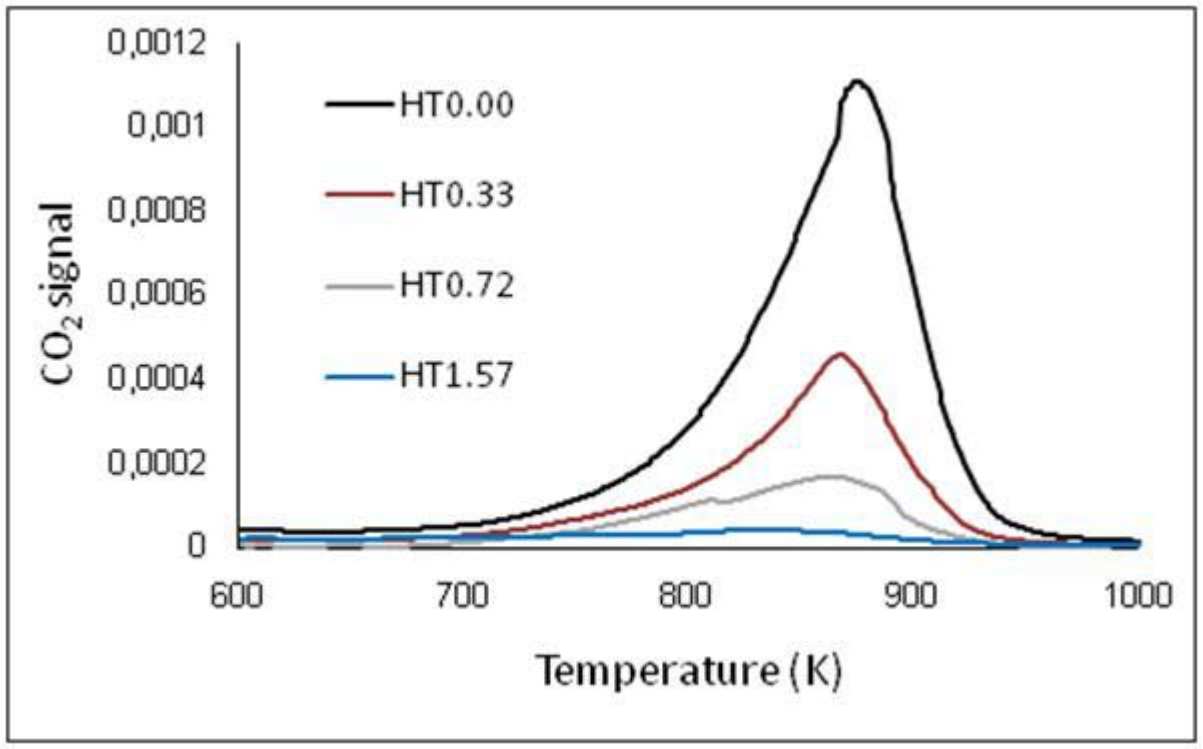
0,0012
0,001
0,0008
0,0006
0,0004
0,0002
0
CO_2 signal
HT0.00
HT0.33
HT0.72
HT1.57
600
700
800
900
1000
Temperature (K)

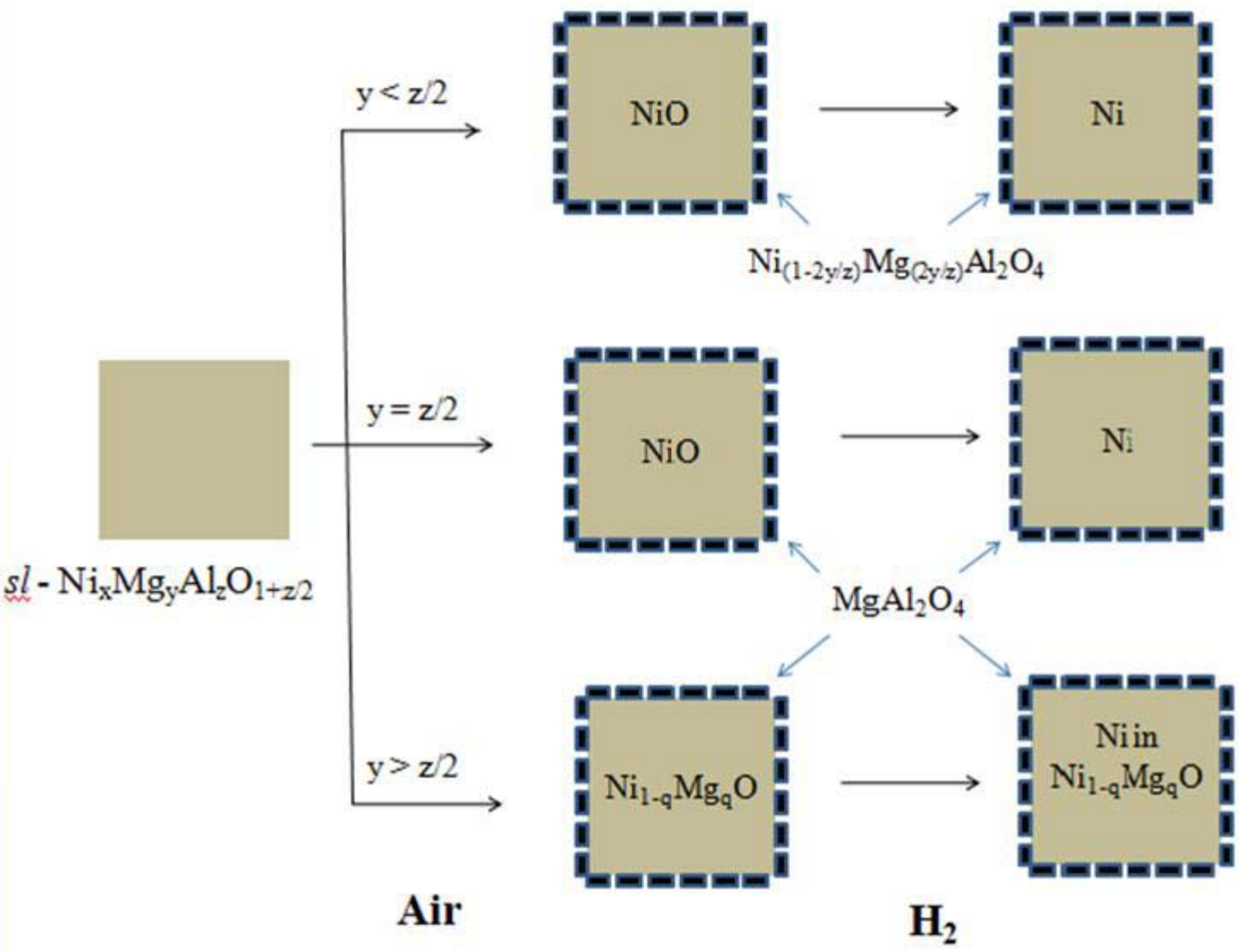
y < z/2
y = z/2
y > z/2
NiO
Ni
$Ni_{(1-2y/z)}Mg_{(2y/z)}Al_2O_4$
NiO
Ni
$MgAl_2O_4$
$Ni_{1-q}Mg_qO$
Ni in $Ni_{1-q}Mg_qO$
sl - $Ni_xMg_yAl_zO_{1+z/2}$
Air
H_2

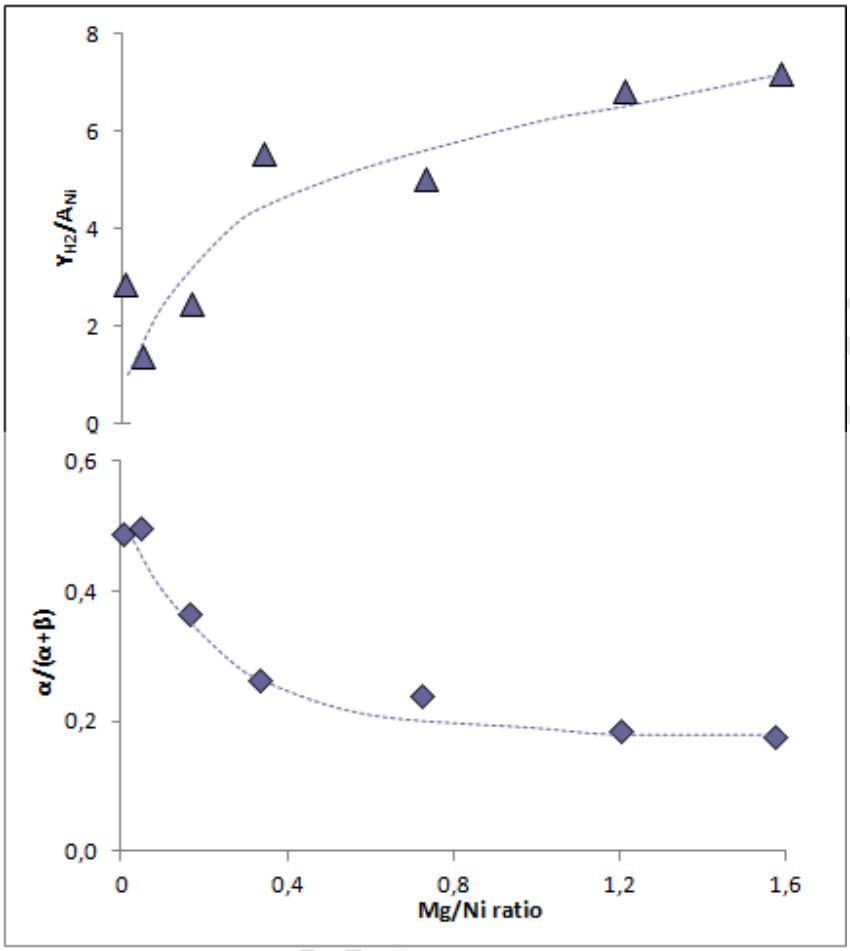

Figura 8.

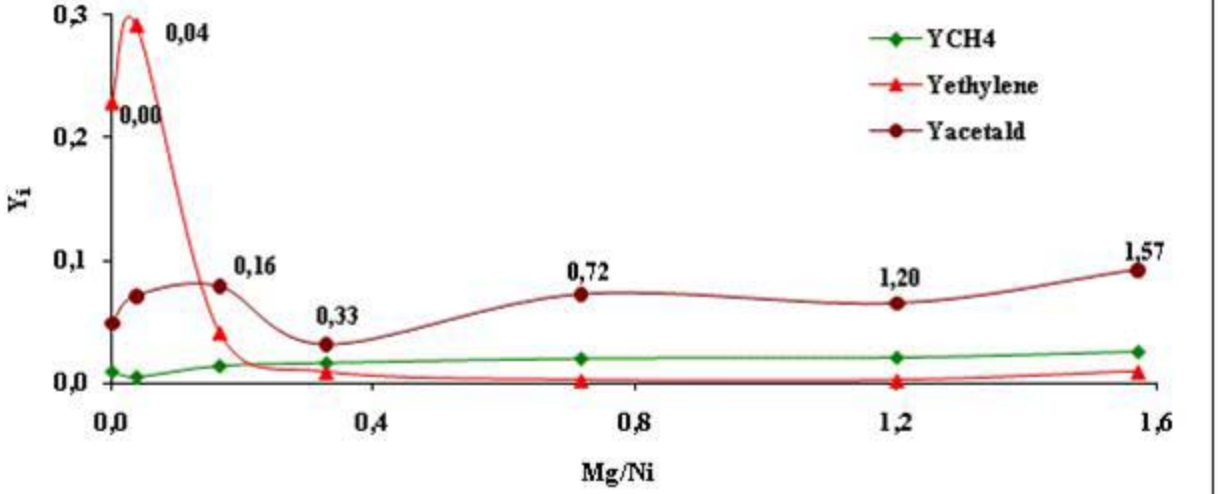
0,3
0,2
0,1
0,0
Yi
0,04
0,00
0,16
0,33
0,72
1,20
1,57
YCH4
Yethylene
Yacetald
0,0
0,4
0,8
1,2
1,6
Mg/Ni

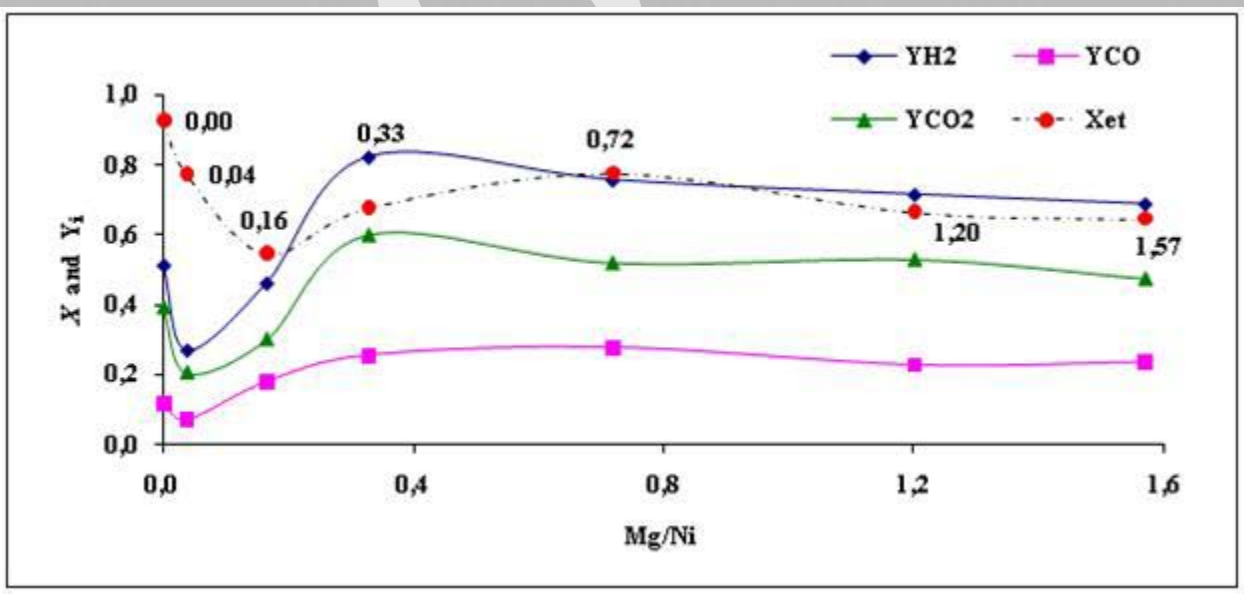
YH2
YCO
YCO2
Xet
1,0
0,8
0,6
0,4
0,2
0,0
X and Yi
0,00
0,04
0,16
0,33
0,72
1,20
1,57
0,0
0,4
0,8
1,2
1,6
Mg/Ni

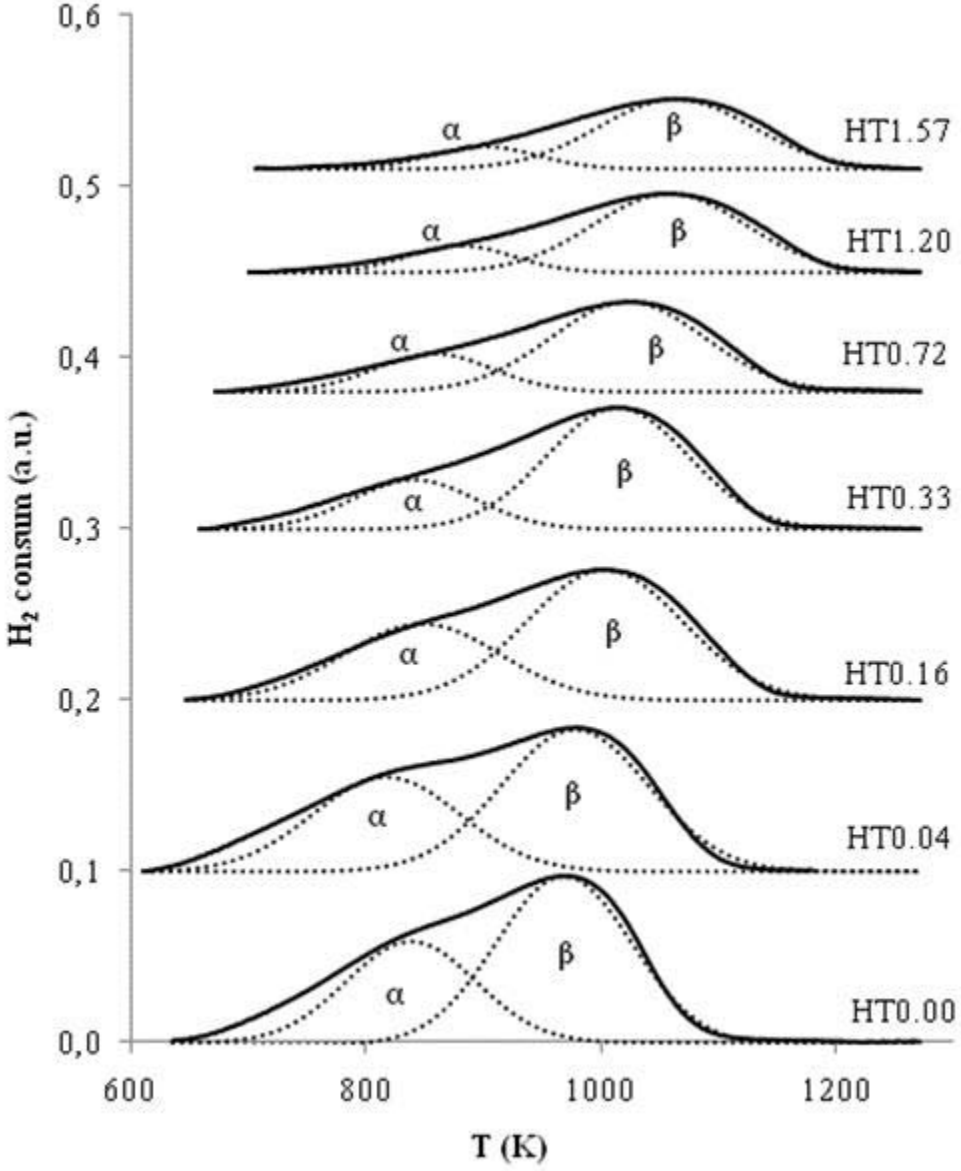
0,6
0,5
0,4
0,3
0,2
0,1
0,0
H2 consum (a.u.)
600
800
1000
1200
T (K)
α
β
HT1.57
HT1.20
HT0.72
HT0.33
HT0.16
HT0.04
HT0.00

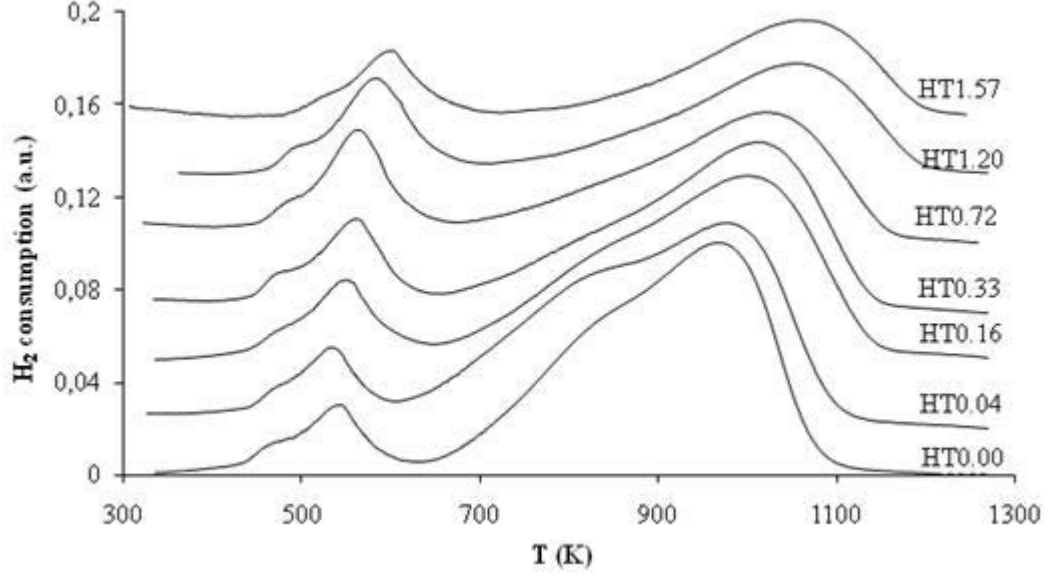
0,2
0,16
0,12
0,08
0,04
0
H2 consumption (a.u.)
HT1.57
HT1.20
HT0.72
HT0.33
HT0.16
HT0.04
HT0.00
300
500
700
900
1100
1300
T (K)

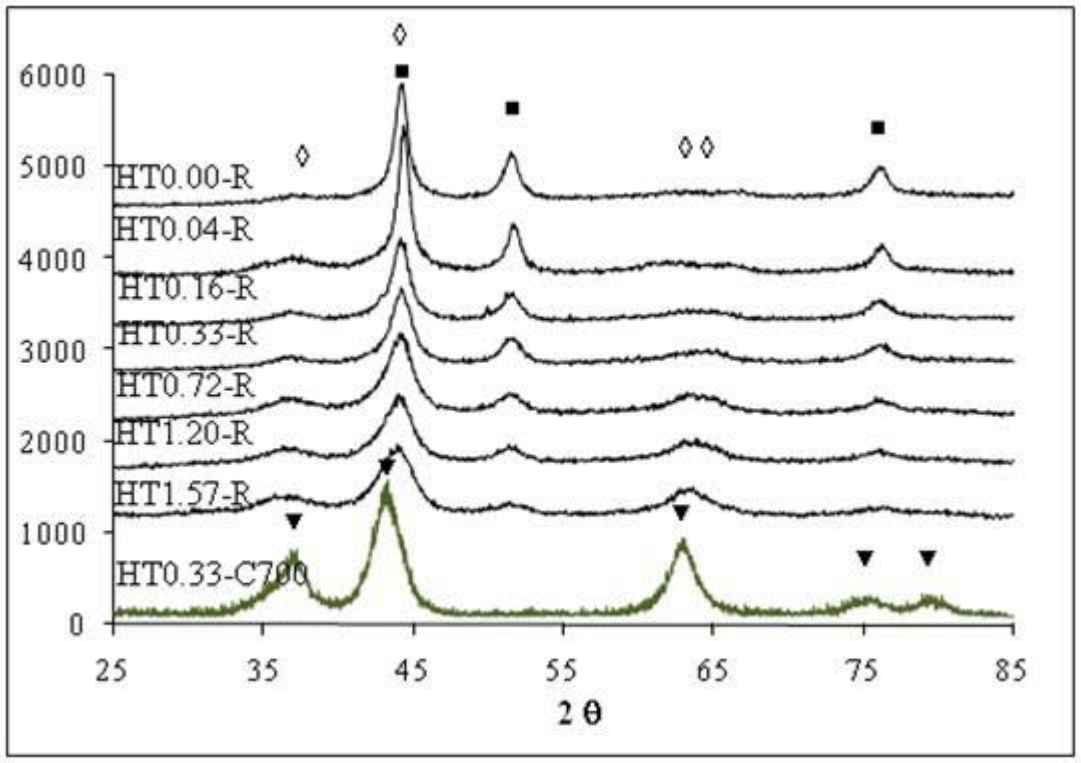
6000
5000
4000
3000
2000
1000
0
HT0.00-R
HT0.04-R
HT0.16-R
HT0.33-R
HT0.72-R
HT1.20-R
HT1.57-R
HT0.33-C700
◊
■
▼
25
35
45
55
65
75
85
2θ

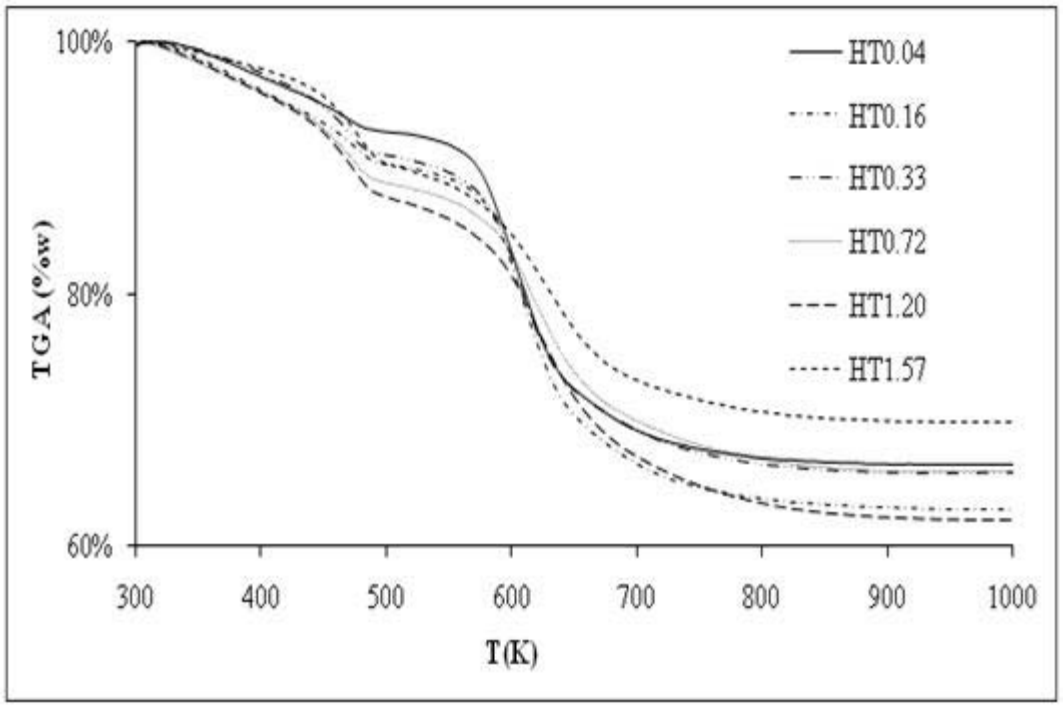
100%
80%
60%
TGA (%w)
300
400
500
600
700
800
900
1000
T(K)
HT0.04
HT0.16
HT0.33
HT0.72
HT1.20
HT1.57

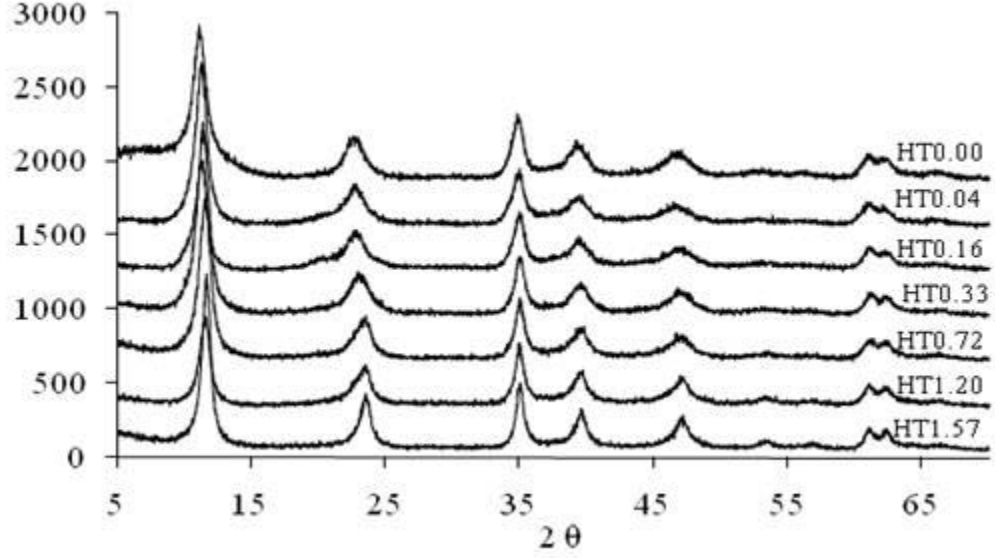
3000
2500
2000
1500
1000
500
0
HT0.00
HT0.04
HT0.16
HT0.33
HT0.72
HT1.20
HT1.57
5
15
25
35
45
55
65
2 θ